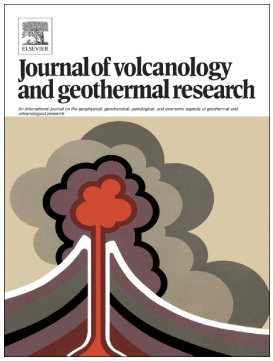
جامعة الملك عبدالله للعلوم والتقنية
King Abdullah University of Science and Technology

Subaqueous hot springs in Köyceğiz Lake, Dalyan Channel and Fethiye-Göcek Bay (SW Turkey): Locations, chemistry and origins

Item Type	Article
Authors	Avşar, Özgür; Avsar, Ulas; Arslan, Şebnem; Kurtuluş, Bedri; Niedermann, Samuel; Güleç, Nilgün
Citation	Avşar Ö, Avşar U, Arslan Ş, Kurtuluş B, Niedermann S, et al. (2017) Subaqueous hot springs in Köyceğiz Lake, Dalyan Channel and Fethiye-Göcek Bay (SW Turkey): Locations, chemistry and origins. Journal of Volcanology and Geothermal Research. Available: http://dx.doi.org/10.1016/j.jvolgeores.2017.07.016.
Eprint version	Post-print
DOI	10.1016/j.jvolgeores.2017.07.016
Publisher	Elsevier BV
Journal	Journal of Volcanology and Geothermal Research
Rights	NOTICE: this is the author's version of a work that was accepted for publication in Journal of Volcanology and Geothermal Research. Changes resulting from the publishing process, such as peer review, editing, corrections, structural formatting, and other quality control mechanisms may not be reflected in this document. Changes may have been made to this work since it was submitted for publication. A definitive version was subsequently published in Journal of Volcanology and Geothermal Research, 7 August 2017. DOI: 10.1016/j.jvolgeores.2017.07.016. © 2017. This manuscript version is made available under the CC-

	BY-NC-ND 4.0 license http://creativecommons.org/licenses/by-nc-nd/4.0/
Download date	24/07/2020 02:23:26
Link to Item	http://hdl.handle.net/10754/625348

Accepted Manuscript



Subaqueous hot springs in Köyceğiz Lake, Dalyan Channel and Fethiye-Göcek Bay (SW Turkey): Locations, chemistry and origins

Özgür Avşar, Ulaş Avşar, Şebnem Arslan, Bedri Kurtuluş, Samuel Niedermann, Nilgün Güleç

PII: S0377-0273(17)30017-3
DOI: doi: 10.1016/j.jvolgeores.2017.07.016
Reference: VOLGEO 6164

To appear in: *Journal of Volcanology and Geothermal Research*

Received date: 4 January 2017
Revised date: 24 July 2017
Accepted date: 24 July 2017

Please cite this article as: Özgür Avşar, Ulaş Avşar, Şebnem Arslan, Bedri Kurtuluş, Samuel Niedermann, Nilgün Güleç , Subaqueous hot springs in Köyceğiz Lake, Dalyan Channel and Fethiye-Göcek Bay (SW Turkey): Locations, chemistry and origins, *Journal of Volcanology and Geothermal Research* (2016), doi: 10.1016/j.jvolgeores.2017.07.016

This is a PDF file of an unedited manuscript that has been accepted for publication. As a service to our customers we are providing this early version of the manuscript. The manuscript will undergo copyediting, typesetting, and review of the resulting proof before it is published in its final form. Please note that during the production process errors may be discovered which could affect the content, and all legal disclaimers that apply to the journal pertain.

ACCEPTED MANUSCRIPT

Subaqueous hot springs in Köyceğiz Lake, Dalyan Channel and Fethiye-Göcek Bay (SW Turkey): locations, chemistry and origins

Özgür Avşar[1*], Ulaş Avşar[2,3], Şebnem Arslan[4], Bedri Kurtuluş[1], Samuel Niedermann[5], Nilgün Güleç[2]

[1]Muğla Sıtkı Koçman University, Department of Geological Engineering, Muğla, Turkey

[2]Middle East Technical University, Department of Geological Engineering, TR-06531, Ankara, Turkey

[3]King Abdullah University of Science and Technology (KAUST), Physical Science and Engineering Division (PSE), Thuwal, Saudi Arabia

[4]Ankara University, Faculty of Engineering, Department of Geological Engineering, TR-06100, Tandoğan, Ankara, Turkey

[5]Deutsches GeoForschungsZentrum GFZ, Telegrafenberg, D-14473 Potsdam, Germany

*Corresponding Author: Muğla Sıtkı Koçman University, Department of Geological Engineering, TR-48000, Kötekli, Muğla, Turkey

Tel (work): +90 252 2113156

Tel (mobile): +90 532 332 9008

Fax: +90 252 211 1912

e-mail: ozguravsar@mu.edu.tr ; ozguravsar@gmail.com

ACCEPTED MANUSCRIPT

ACCEPTED MANUSCRIPT

ABSTRACT

In this study, horizontal temperature measurements along organized grids have been used to detect subaqueous hot springs. The study area, located in the southwest of Turkey and comprised of Köyceğiz Lake, Dalyan Channel and Fethiye-Göcek Bay, was scanned by measuring temperatures horizontally, 2-3 meters above the bottom of the lake or sea. After analyzing the temperature data along the grids, the locations with anomalous temperature values were detected, and divers headed here for further verification. Accordingly, among these anomalies, the divers confirmed seven of them as subaqueous hot springs. Three of these hot springs are located in the Köyceğiz Lake, three of them are located in the Dalyan Channel and one hot spring is located in the Fethiye-Göcek Bay. At the locations where temperature anomalies were detected, the divers collected samples directly from the subaqueous hot spring using a syringe-type sampler. We evaluated these water samples together with samples collected from hot and cold springs on land and from local rivers, lakes and the sea, with an aim to generate a conceptual hydrogeochemical model of the geothermal system in the study area. This model predicts that rainwater precipitating in the highlands percolates through fractures and faults into the deeper parts of the Earth's crust, here it is heated and ascends through the sea bottom via buried faults. Pervious carbonate nappes that are underlain and overlain by impervious rocks create a confined aquifer. The southern boundary of the Carbonate-Marmaris nappes is buried under alluvium and/or sea/lake water bodies and this phenomenon determines whether hot springs occur on land or subaqueous. The chemical and isotopic properties of the hot springs point to seawater mixing at deep levels. Thus, the mixing most probably occurs while the water is ascending through the faults and fractures. The gas geochemistry results reveal that the lowest mantle He contributions occur in the samples from Köycegiz Lake, whereas the highest ones are found in samples from the Dalaman plain. For the first time, we made use of the micro-XRF sediment core scanning (ITRAX Scanner) for

ACCEPTED MANUSCRIPT

exploring the relation between subaqueous geothermal occurrence and chemical properties of the surrounding sediments. The spatial elemental distribution of sea/lake bottom sediments suggests that depending on the surrounding rock units and the temperature of the hot spring, the sediments around the spring can be enriched with certain elements.

Key words: Water chemistry, Mixing, Gas geochemistry, ITRAX analysis, Saturation index, Conceptual model

1. Introduction

The world's energy demands are increasing (IEA, 2012) along with the global population and resulting rise in consumption, which in turn leads to further exploration of alternative and renewable energy sources by investors, researchers, and governments. Geothermal energy production has become popular since it is environmentally friendly when compared to stock-limited fossil fuels and the emissions of greenhouse gases associated with their burning. Along with the limited environmental concerns associated with geothermal energy, its sustainability will likely make it an indispensable energy source in the future.

Most of the on-land geothermal sites in Turkey are well studied. For example, there were a number of comprehensive studies carried out about the hydrogeochemistry of Turkish on-land geothermal sites (İlkışık, 1995; Balderer and Synal, 1997; Mutlu and Güleç, 1998; Vengosh et al., 2002; Tarcan, 2005; Süer et al., 2008; Baba and Sözbilir, 2012; Bundschuh et al., 2013; Karakuş and Şimşek, 2013; Özgür and Çalışkan, 2013). In addition, there exists an inventory of the geothermal sites issued by the General Directorate of Mineral Research and Exploration (MTA) in 2005. Tüfekçi et al. (2010) used this inventory together with the publicly available magnetic anomaly, Bouguer gravity anomaly, earthquake epicenter and lineament datasets and statistically showed the spatial distribution of potential geothermal occurrences in western Anatolia.

ACCEPTED MANUSCRIPT

Geothermal energy started gaining popularity in Turkey after a geothermal law was passed in 2007. Accordingly, geothermal investments in electrical power generation increased by 336% (Bertani, 2015), and the direct utilization of geothermal energy increased by 38% over the last five years (Mertoğlu et al., 2010; Mertoğlu et al., 2015). Moreover, the purchasing guarantee issued by the Turkish Government at a rate of 0.105 USD/kWh has provided the sector with a great incentive for investment. Mertoğlu et al. (2015) reported that there are over 2000 hot and mineral water sources, and 227 geothermal sites in Turkey, 70-80% of which are located in western Anatolia.

Not only in Turkey but also throughout the world, on-land geothermal sources have witnessed extensive exploration through geochemical, mineralogical, and hydrogeochemical investigations as well as expensive geophysical prospecting methods such as seismic stratigraphical methods. However, explorations for subaqueous geothermal resources have not yet had their deserved attention. There have been efforts to estimate the earth's heat loss and to assess shallow hydrothermal activity. For example, Williams (1976) stated that approximately 2×10^{12} cal/s ($=8.37\times10^{12}$ W) of heat (20% of the earth's heat loss) is released through 1% of the Earth's surface area. This release is in the form of hydrothermal discharge from young rocks near active seafloor-spreading areas and submarine volcanoes. This amount of energy was roughly equal to the world's total energy consumption at that time (1976). Similarly, Prol-Ledesma et al. (2005) described "shallow hydrothermal activity" as an interesting but not-as-yet well-studied phenomenon, where shallow means a water depth less than 200 m, and they stated "Shallow-water vents provide accessible geological and chemical settings for studying the interaction of hydrothermal fluids with unconsolidated sediments, seawater, and basement rocks". More recently, Suarez-Arriaga et al. (2014) declared that submarine geothermal resources have not been sufficiently used and studied yet, but they could cover the world's considerable energy demand of in an environmentally friendly way

ACCEPTED MANUSCRIPT

by integrating on-land geothermal prospecting experience and offshore hydrocarbon exploitation technology.

Although submarine and sub-lacustrine hydrothermal systems are not as well studied as on-land geothermal sources, recent technological developments have drawn many researchers to undertake studies on subaqueous hydrothermal systems. These studies include the ones carried out in lakes (Michel et al., 2001; Remsen et al., 2002; Ronde et al., 2002; De Batist et al., 2002; Duchkov et al., 2009), and in different parts of the world including Greece, Italy, Japan, the Antilles, Galapagos rift zone, Iceland, Mexico, the Pacific Ocean, Papua New Guinea, and Turkey (Williams et al., 1974; Corliss et al., 1979; Italiano and Nuccio, 1991; McMurtry et al., 1993; Michard et al., 1993; Fitzsimons et al., 1997; Hannington et al., 2001; Glasby and Notsu, 2003; Prol-Ledesma, 2003; Prol-Ledesma et al., 2004; McCarthy et al., 2005; Pichler, 2005; Valsami-Jones et al., 2005; Esposito et al., 2006; Koschinsky et al., 2007; Pekçetinöz et al., 2009; Arango-Galván et al., 2011; Yamanaka et al., 2013). However, most of the hydrothermal systems in these studies were either discovered by chance or identified by local people.

This study presents the results of the exploratory research of subaqueous thermal systems that were expected to occur at the bottom of Fethiye-Göcek Bay as well as the Köyceğiz, Alagöl, Sülüngür and Kocagöl lakes (Fig. 1), according to the measurements of water temperature along horizontal lines taken to detect temperature anomalies. In addition, a hydrogeochemical conceptual model of the region was constructed by using water, gas and sediment geochemistry. The study area is located in southwestern Anatolia, which is a seismically active region. Additionally, the Fethiye-Göcek shoreline is located along one of the main fault zones of SW Anatolia, namely, the Fethiye-Burdur fault zone (on land continuation of Pliny-Strabo fault zone) (Fig. 1). There are lineations recorded by Yağmurlu et al. (2005), Ocakoğlu (2011) and faults recorded by Hall et al. (2014) in the south of continental shelf of Fethiye-

ACCEPTED MANUSCRIPT

Göcek Bay. Findings of these researches favor the idea that there are submarine buried faults at the bottom of the Fethiye-Göcek Bay, these may enable submarine geothermal systems, making the Fethiye-Göcek Bay a potential site to investigate for submarine hot springs.

2. Geological setting

The Menderes Massif, the Beydağları Autochthon and the Lycian nappes are the main tectonic units of SW Anatolia (Fig. 1). The study area is located mainly on the Lycian nappes; the Beydağları Autochthon crops out in the region as tectonic windows. The Beydağları Autochthon is composed of Upper Cretaceous carbonate rocks and is the base rock in the region. The Lycian nappes are thrusting over the Beydağları Autochthon tectonically. Although there are many categorizations for the Lycian nappes, in this study we mainly use the one of Şenel (1997a; 1997b) where the nappes are divided into 5 main units: the Yeşilbarak, Tavas, Bodrum, Gülbahar, and Marmaris Nappes from the bottom to the top (Fig. 1).

The Late Lutetian-Early Burdigalian aged Yeşilbarak nappe is composed of shales and sandstones and located between the Beydağları Autochthon and the overlying Lycian nappe units. The overlying Tavas, Bodrum and Gülbahar nappes are composed of carbonate units and presented together (without differentiating) in the geological map as their hydrogeological properties are similar in the region. The Lower Cretaceous Marmaris nappe comprising peridotites overlies all rock units in the region and crops out as a NW-SE trending strip. The impervious to semi-pervious character of this unit greatly affects the hydrogeology, and consequently the geothermal system of the region. This subject matter will be discussed in the Hydrogeochemical Model section (Section 4.4.4) in detail.

3. Materials and methods

ACCEPTED MANUSCRIPT

In order to detect the temperature anomalies, we measured the temperature of the water together with electrical conductivity (EC) and pH along horizontal linear routes. Where temperature anomalies were detected, divers were sent to these localities to seek and confirm the presence of the hot springs. If there was a hot spring, water samples were taken, to be analyzed chemically. Together with the subaqueous samples, on-land hot and cold springs, stream water, seawater, lake water and channel water were sampled and chemically analyzed. The results of these chemical analyses were used to develop a hydrogeochemical model. Along with water chemistry, we also studied gas and sediment geochemistry. The following subsections present further details.

3.1 Subaqueous hot spring exploration/prospecting

In order to explore subaqueous hot springs in the study area, a total of about 900 km of cruising was carried out (Fig. 2), using a boat equipped with a sonar-mounted Global Positioning System (GPS) device (Garmin GPSmap 421s) and a multi-parameter conductivity-temperature-depth (CTD) sonde (YSI 6600), which allowed simultaneous real-time measurements of geographical coordinates, water depth and temperature. During the cruising, based on the water depth information from the sonar, the CTD was lowered down to a certain height above the sediment/water interface (2-3 m), and its depth was modified with respect to the bathymetrical changes. In this way, we ensured that we measured the water temperature as close as possible to the probable subaqueous hot springs while preventing the CTD from crashing to the ground. By setting the cruise speed to ca. 7 km/h and the devices to perform measurements every two seconds, we also ensured that the CTD and GPS measurements were done every 4 meters along the cruising routes. As a preliminary approach, the routes were designed in order to cover the complete target area of the bay and lakes. After analyzing the data, promising sites were identified, and more detailed measurements were done around these locations via fine grid routes.

ACCEPTED MANUSCRIPT

In order to detect water temperature anomalies, which could be related to subaqueous hot springs, the datasets from the CTD and GPS were merged and synchronized to obtain temperature vs. time plots. Careful inspection of those plots allowed the determination of the approximate locations of the "potential" subaqueous hot springs. Afterwards, more detailed exploratory cruises with denser survey grids were conducted at the "potential" locations in order to confirm the anomalies and to provide the divers with more precise coordinates for water sampling. While measuring the temperature, EC and pH, sonar profiles were taken by the GPS. These sonar profiles were recorded by taking screenshots from the GPS device, and they were investigated and used as a tool to detect subaqueous hot springs. Moreover, some topographic anomalies, which may be related to the faults, were detected using the detailed bathymetric data generated by sonar GPS measurements. The CTD measurements were concentrated around these locations by designing a finer cruise grid.

3.2 Hydrochemistry

Whenever the divers confirmed the presence of a hot spring, they collected water samples with syringe-type samplers, measured the temperature of the spring water by putting the CTD at the outlet of the hot spring, and took photos as well as videos. The water samples were collected directly from the outlet of the spring to avoid or minimize mixing with sea/lake water. The water samples in the syringes were transferred into three different polyethylene bottles (100 ml each) for stable isotope, cation+trace element, and anion analyses, respectively.

Samples collected for cation and anion analyses passed through a 0.45 μm filter, and the former ones were acidified to 1% HNO_3 after filtering. Along with subaqueous hot spring samples, five on-land fresh water springs were also sampled (Fig. 1). In addition, three water samples were taken from the sea surface in order to delineate the chemical and isotopic

ACCEPTED MANUSCRIPT

properties of the seawater (Table 1). The water samples were kept refrigerated (4 °C) and immediately sent to dedicated laboratories. Major ion and trace element analyses were carried out at the Hacettepe University Water Chemistry and Environmental Tritium Laboratory (Ankara, Turkey), and stable isotope analyses were carried out at the Hacettepe University International Karst Water Resources Application and Research Center Stable Isotope Laboratory (UKAM, Ankara, Turkey). The titration technique was used to determine carbonate (CO_3^{2-}) and bicarbonate (HCO_3^-) ion concentrations. Fluoride (F^-), chloride (Cl^-), nitrite (NO_2^-), bromide (Br^-), nitrate(NO_3^-), phosphate (PO_4^{3-}), sulfate (SO_4^{2-}), lithium (Li^+), sodium(Na^+), ammonium (NH_4^+), potassium (K^+), magnesium (Mg^{2+}), and calcium (Ca^{2+}) ion concentrations were determined by using a high performance ion chromatography device (DIONEX LC25, ICS-1000 Ion Chromatography system) and a conductivity detector. The spectrophotometric method (aT60U Spectrometer) was used to determine SiO_2 and boron concentrations. Trace element (Ag, Al, As, Au, Ba, Be, Cd, Ce, Co, Cr, Cs, Cu, Dy, Er, Eu, Fe, Ga, Gd, Ge, Hf, Hg, Ho, Ir, La, Lu, Mn, Mo, Nb, Nd, Ni, Pb, Pd, Pr, Pt, Rb, Re, Rh, Ru, Sb, Se, Sm, Sn, Sr, Ta, Tb, Te, Th, Ti, Tl, Tm, U, V, W, Y, Yb, Zn, Zr) concentrations were measured in a Thermo Electron X7 model ICP-MS (Inductively Coupled Plasma–Mass Spectrometer) and the detection limits range between 0.001 ppt to 0.3 ppb. Chemical analyses of the waters were conducted in compliance with Clesceri et al. (1989). Stable isotope analyses were conducted by using laser spectroscopic methods, where the reference standard was Vienna Standard Mean Ocean Water (VSMOW). The analytical precisions are 0.2‰ and 1‰ for $\delta^{18}O$ and δD, respectively.

Helium analyses of eleven samples were conducted at the GFZ Potsdam noble gas laboratory in Germany. Four of those samples were collected from subaqueous springs, and seven of them from on-land springs. At seven locations, including the subaqueous spring SUBC-2, free gas bubbling through the water was collected in glass flasks by means of a funnel, while at

ACCEPTED MANUSCRIPT

four locations spring water was sampled in 1 cm outer diameter, 50 cm long copper tubes sealed by steel clamps. During sampling, special care was taken to avoid atmospheric contamination. Except for the gas sample SUBC-2 (see above), the other subaqueous springs were sampled by installing a small water pump at the outlet of the spring. In the lab, total gas analyses were carried out for the free gas samples using a Pfeiffer Omnistar quadrupole mass spectrometer. Detection limits in these analyses are ~10 ppmv for N_2, O_2, CO_2, and ~1 ppmv for H_2 and Ar (Wiersberg et al., 2011). The glass flasks were then attached to the noble gas line, and appropriate volume splits were analyzed for noble gas concentrations and isotopic compositions. Water samples from copper tubes were discharged into a glass bulb and degassed in an ultrasonic bath, and the gases were transferred to a cold trap by means of a laminar flow of gaseous H_2O (evaporated from the liquid water sample) through a connecting capillary. Again, appropriate splits were transferred to the noble gas line. There, chemically active gases were removed using another cold trap, two Ti sponge getters, and two SAES (Zr-Al) getters, and the noble gases were adsorbed to a stainless steel frit or activated charcoal in two cryostatic cold heads in order to separate them from each other for the measurement in a VG5400 noble gas mass spectrometer. Further details about experimental procedures and data reduction methods can be found in Niedermann et al. (1997).

3.3 Sediment geochemistry

In order to spatially evaluate the geochemical composition of the bottom sediments, and therefore in order to detect the possible geochemical effects of subaqueous hydrothermal fluid emissions on sedimentation, gravity cores were collected and analyzed by an ITRAX μXRF core scanner. For an unbiased spatial comparison, it is crucial to do the geochemical analyses for the same stratigraphical horizon (i.e., on the sediments that were deposited in the same time window). For this reason, this study targeted the sediments at the water/sediment

ACCEPTED MANUSCRIPT

interface. Accordingly, rather than using an Ekman sampler that may significantly mix and disturb sediments, we used a gravity corer with a messenger-triggered vacuum system. Moreover, this method helped to achieve minimum sediment loss and disturbance at the water/sediment interface.

A total of 233 gravity cores, 30-50 cm long, with a diameter of 7.5 cm, were collected (99 from Fethiye-Göcek Bay, 105 from Köyceğiz Lake, and 29 from Dalyan Channel). The cores were collected in two groups: 1) Cold Location Cores (CLC), which were almost uniformly distributed within the study areas to reveal the general characteristics of sediments, and 2) Hot Location Cores (HLC), which were collected in the vicinity of the detected subaqueous hot springs. The geochemical data from the CLCs and HLCs were then compared to investigate the possible effects of subaqueous hot springs on the chemical composition of sediments.

Since splitting and scanning 233 cores one by one would require a significant amount of labor and time, only the top 3-5 cm of each gravity core were sampled by using 2 cm diameter syringes, and put successively in PVC half pipes. In this way, ten artificial cores, being approximately 1 m long and containing sediments from 20-30 locations each, were prepared and sent to the GEOPOLAR Laboratory of the University of Bremen for ITRAX μXRF scanning to obtain geochemical data as well as optical and radiographic images.

Along the artificial cores, radiographic scanning was done at 200 μm resolution. XRF scanning, on the other hand, was carried out with a Mo-tube at 1 mm increments for the Fethiye-Göcek cores, and at 2 mm increments for the Köyceğiz and Dalyan cores, with an exposure time of 12 seconds. As a result of the XRF scanning, semi-quantitative distributions of 19 elements (Si, S, Cl, K, Ca, Ti, Cr, Mn, Fe, Ni, Zn, As, Se, Br, Rb, Sr, Y, Zr, and Pb) were obtained in units of kilo counts per second (kcps). For each element, average values for all sampling locations were calculated. In order to achieve comparable scales among the

ACCEPTED MANUSCRIPT

elements for spatial evaluation, average kcps values were standardized separately for the three study sites, which have different sedimentological environments.

Since ITRAX μXRF scanning is performed on bulk sediments, the scanning results are also influenced by the physical properties of the sediments, such as grain-size distribution, water, and organic matter contents. In order to minimize these effects and to better reveal the geochemical signal, inter-element ratios are used (e.g., Croudace et al., 2006; Kylander et al., 2011). As a first step, all possible inter-element ratios (i.e., 380 for 19 elements) were calculated for each location and their spatial distribution maps were prepared. However, visual inspection of spatial distribution maps does not always reveal the difference between the HLCs and CLCs. For this reason, the mean values of inter-element ratios from the two groups of cores (i.e., HLCs and CLCs) were determined and compared. Finally, those inter-element ratios of the HLCs that significantly deviated from the means of the CLCs were detected and were attributed to the effect of subaqueous hot springs on the chemical composition of the sediments.

4. Results and discussions

4.1. Subaqueous hot spring exploration/prospecting

The measurement routes and the bathymetric maps are shown in Fig. 2. Along with the temperature measurements, EC and pH values were also measured. As a result of these physicochemical measurements, on first inspection of the data, over one hundred temperature anomaly indications were detected (some of the selected anomalies can be seen in time vs. temperature plots provided in Supplementary Fig. 1). At several of these locations, detailed physicochemical measurements were performed by tracking along a finer mesh of routes (Fig. 2a and b). As a result, divers were sent to 49 potential hot spring locations for confirmation of the presence of subaqueous hot springs. Among the 49 locations, they confirmed seven

ACCEPTED MANUSCRIPT

subaqueous hot springs: three in Köyceğiz Lake, three in the Dalyan Channel, and one in the Fethiye-Göcek Bay (Fig. 1). The temperature of the subaqueous hot springs in the Köyceğiz Lake ranges between 26.17 and 29.47 °C (Table 1). The discharge temperatures of the Dalyan subaqueous springs are around 27-28 °C. The water depth and temperature of the subaqueous hot spring in the Fethiye-Göcek Bay was 19 m and 27.19 °C, respectively (VIDEO). No temperature anomalies were found at the bottom of the Alagöl, Sülüngür and Kocagöl lakes.

The other aid used in detecting hot springs were the sonar profiles. SUB-2 and SUB-3 springs in Köyceğiz Lake were detected by considering the lineations on the sonar profile as an indication of a subaqueous hot spring. These locations were also marked as anomalies, and divers were sent there in order to search for the hot springs under water. Bathymetry maps of Köyceğiz Lake and the Fethiye-Göcek Bay were prepared by using the sonar GPS data (Fig. 2c and d). Köyceğiz lake has two troughs in the north and the south and the deepest points are 25 m and 32 m respectively. In the Fethiye-Göcek Bay the shelf is located around 125 m from the shoreline, and the water depth reaches 500 m in the outer shelf. Some lineations were detected in the bay through detailed investigation of the bathymetry map; they may be inferred as the faults at the bottom of the sea. Temperature anomalies that were detected at the nearshore section of these lineations made these areas potential subaqueous hot spring sites, so it was worth studying them in detail (Fig. 2b). Except for İnlice Bay, there were, however, no hot springs found at the remaining three locations.

4.2 Sediment geochemistry

ITRAX μXRF scanning on basin-wide sediment samples allowed detection of the geochemical traces of subaqueous hot springs on the sediments. The locations of the cores collected in this study are presented in Fig. 3. The optical and radiographic images of the artificial cores, which are composed of the top 3-5 cm of sediment from 233 gravity cores, are

ACCEPTED MANUSCRIPT

shown in Supplementary Fig. 2. Along the radiographic images, especially, the boundaries between different cores can be clearly seen as horizontal white lines, which correspond to mm-scale low-density gaps. Before calculating the average "kcps" values for each element at coring locations, several measurement points above and below these boundaries are excluded from the XRF dataset since they can be erroneous. After data purging, the average "kcps" values were standardized for each element in the three study sites separately (Köyceğiz Lake, Supplementary Table 1; Dalyan Channel, Supplementary Table 2; and Fethiye-Göcek Bay, Supplementary Table 3).

All possible elemental ratios derived from the standardized "kcps" values are plotted separately for the cold and hot locations of each site (Supplementary Fig. 3). In addition, these ratios are interpolated over the study areas to visualize their spatial distribution (Supplementary Fig. 4). Fig. 5 illustrates the Sr/Ti ratios at the coring locations in the Fethiye-Göcek Bay. The cores are sorted along the x-axis in the way that the 12 HLCs are plotted far-left in the graph and the CLCs in the order roughly from west to east (Fig. 4a). It is clear from the plot that the mean Sr/Ti ratio of the HLCs significantly deviates from the CLCs and is almost 4σ higher than the mean of the CLCs. The spatial distribution map of the same ratio, on the other hand, enables visualization and can pinpoint the highest values of the HLCs (Fig. 4b). This observation implies that the sediments around the subaqueous hot spring in İnlice Bay are enriched in Sr. It should also be noted that the high Sr/Ti ratio of the F-71 core, which was classified as CLC, may indicate another hot spring location in the vicinity of that core. Unfortunately, water sampling could not be done at this location since the depth is around 40 m there, which exceeds the safe diving limit.

Similar to the Sr enrichments illustrated in Fig. 4, other elemental enrichments were also detected. In order to find out which elements are more prominent, the deviations of the HLCs from the CLCs for all possible elemental ratios are presented in matrix form for the three

ACCEPTED MANUSCRIPT

study sites separately (Fig. 5). The colors of the cells represent the magnitude of deviation between the means of CLCs and HLCs. For instance, in Köyceğiz Lake, the means of the ratios of Cl to almost all other elements for HLCs are higher by 2σ than the mean of the same ratios for CLCs. It can be deduced, accordingly, that the sediments around the Köyceğiz subaqueous hot springs are enriched in S, Cl, and Br, while they are depleted in Mn (Fig. 5a). Similarly, in the Fethiye-Göcek Bay, the sediments around the subaqueous hot spring in İnlice Bay are enriched in S, Cl, Ca, and Sr (Fig. 5c). No significant elemental enrichment related to subaqueous hot springs is detected in the Dalyan Channel (Fig. 5b). The plots and some of the representative spatial distribution maps for the above-mentioned elements are presented for Köyceğiz Lake and Fethiye-Göcek Bay in Fig. 6. In Köyceğiz Lake, not only the HLCs but also the CLCs in the southern basin show similar anomalies, which implies that the subaqueous hot springs affect the sedimentation throughout the southern basin. This can be attributed to the lack of significant tributaries in the southern basin, which may cause subaqueous hot springs to dominate the water chemistry in the basin.

Although some elemental ratios show significant anomalies in the Köyceğiz Lake and the Fethiye–Göcek Bay, no prominent elements could be determined for the Dalyan Channel. The absence of any elemental enrichment in the Dalyan Channel can be due to water currents in the channel, which may hinder regular sedimentation, thereby preventing any archive of sedimentary traces of subaqueous hot springs on the channel's bottom sediments.

4.3 Hydrogeochemistry

4.3.1 Water chemistry

For a better understanding of the origin of natural waters, it is crucial to characterize their chemical properties in detail. Major and minor ion concentrations of the waters are given in Table 2 and Table 3, respectively. According to the results, inland cold waters and stream

ACCEPTED MANUSCRIPT

waters are of the Mg or Ca – HCO_3 type (Fig. 7). The other samples (subaqueous, lake, channel etc.) are Na-Cl type waters. This is an expected result because a seawater contribution to the lake waters and geothermal waters in the Köyceğiz-Dalaman region was reported by previous studies (Bayarı et al., 1995; Gökgöz and Tarcan, 2006; Avşar et. al., 2016). The total dissolved solids (TDS) of the waters range from 302 to 41528 ppm. When the Cl ion concentration and TDS are compared, it is obvious that the TDS of the waters are dominated by the Cl concentration (Fig. 8). The Cl content of the waters may be considered as seawater contribution. Accordingly, it is obvious that all the waters (including subaqueous springs) are mixtures of fresh and seawater, and the seawater contribution (Cl concentration) correlates with the distance to the sea. This phenomenon will be the key point of the hydrogeochemical model, which will be discussed in the following sections.

In order to find out the possible impacts of temperature on mineralization, Saturation Indices (SI) were calculated by changing the temperature from 20 to 165 °C with the help of the computer program PHREEQC (Parkhurst and Appelo, 1999). The results for SUB-1 and SUB-7 are presented as temperature vs SI graphs in Fig. 9. In the Fethiye-Göcek Bay, the calculated SI of the SUB-7 hot spring in İnlice Bay reveals that aragonite, calcite, dolomite, and fluorite are highly saturated (positive SI) at the discharge temperature of the hot spring (i.e., 28 °C) (Fig. 9a). Hence, the Ca enrichments at this spot can be attributed to precipitation of the above-mentioned minerals from SUB-7 hot spring water. Sr has similar chemical properties as Ca, and thus it can replace Ca within the crystalline structure of the above-mentioned minerals (Hem, 1985). Sr is a trace element and is not as abundant in nature as Ca. Yet, given their chemical similarities, it is not unusual to observe Sr anomalies in a system with Ca anomalies. The mineral anhydrite, the presence of which could be a possible explanation for high S values in İnlice Bay sediments, has positive SI values at temperatures higher than 80 °C. Given the discharge temperature of 28 °C, the SI of anhydrite for the İnlice

ACCEPTED MANUSCRIPT

Bay hot spring is negative, which eliminates the possibility of S-enrichment due to anhydrite precipitation. The presence of S and Sr anomalies may also be due to celestite precipitation; however, its SI is also negative at all temperatures and hence, it is not likely that the high abundances of these elements are related to this mineral. Although the present chemical composition of the İnlice Bay hot spring does not seem suitable for anhydrite and celestite precipitation, it might have been different in the recent past. Given that the elemental results are the average values of the top 3-5 cm of the sediments, which represents ca. 15-20 years of sedimentation, S and Sr enrichments may indicate that the chemical composition of the İnlice Bay hot spring was possibly different and was suitable for anhydrite and celestite precipitation in the past.

It is well known that the Cl ion is highly soluble, thus it is almost impossible for Cl to make a bond with a cation and precipitate as a mineral once it enters the solution as an anion. Hence, highly negative saturation values of sylvite and celestite are not surprising in this study. To explain Cl enrichments in the sediments, a more extended and comprehensive study focusing on geochemistry is required.

Cl and Br enrichments in the sediments around the Köyceğiz subaqueous spring cannot be explained by halite or sylvite precipitation since their saturation index values are highly negative (Fig. 9b). In order to find out the reason for Cl and Br-enriched sediments, more detailed investigations and analyses such as pore water chemistry analyses are required in this area.

4.3.2 O- and H-isotope compositions

Stable isotope ratios are useful to understand the origin of the waters and delineate the subsurface processes that affect their chemical composition. In this study, two campaigns of sampling were conducted for stable isotope analyses; 1) in September 2013 (dry season) and

ACCEPTED MANUSCRIPT

2) in May 2014 (wet season) (Table 4). Highly negative δD and $\delta^{18}O$ values of on-land fresh waters are an indication of recharge from inland and high altitudes (Fig. 10a and b). The on-land fresh waters seem to be of meteoric origin. However, a seawater effect is obvious where the $\delta^{18}O$ and δD values of the affected waters plot on a line that connects fresh water and seawater instead of the meteoric water lines (Fig. 10 a and b). This line may be interpreted as a mixing line between the freshwater and the seawater in the study region.

Another point that should be mentioned here is the role of the geographic position of the sampling locations (waters) with regard to seawater contribution. The closer the sampling location is to the sea, the more positive the isotope ratio becomes. As mentioned above, the mixing phenomenon was inferred from the chemical composition (Cl concentration) of the waters, and the distance to the sea affects the amount of seawater contribution and thus the Cl concentrations. The waters from close to the sea are also enriched with heavy isotopes, while the distant ones mostly show properties similar to fresh waters and are enriched in light isotopes.

The seasonal variations in the stable isotope ratios are also an important point to be taken into account. The water samples are generally, slightly enriched in light isotopes of O and H during the wet season (Fig. 10a). The most probable reason for this is a dilution effect due to the contribution of rainwater, which is enriched in light isotopes. On the other hand, during the dry season the waters are enriched in heavy isotopes of O and H, most probably due to evaporation. There are two samples which do not follow the seasonal variation trend: 1) Sülüngür Lake water and 2) sample DAL-2 from the Dalyan Channel (Table 4, Fig. 10b). The Dalyan Channel and Sülüngür Lake are known to be connected to the sea. A heavy isotope enrichment (seawater effect) in these waters in the wet season, in spite of the diluting effect of rainwaters, may be due to a water current that occurs in the wet season from the sea to the

ACCEPTED MANUSCRIPT

lake and channel. Although Alagöl Lake is also connected to the sea in the same way, a light isotope enrichment in this lake's waters in the wet season is compatible with the other waters. This indicates that although Alagöl Lake is very close to the sea and connected to it by a channel like Sülüngür Lake, for some reason, it is physically more isolated.

4.3.3 Gas geochemistry

The geothermal potential is generally high in areas where there is recent magmatic or tectonic activity like volcanism, extension, or fluid transport through fault-hosted deep pathways. The most sensitive indicator of such activity is the isotopic composition of helium ($^3He/^4He$) (e.g. Kennedy and van Soest, 2007). Variations in helium isotope ratios of the fluids give researchers clues about the origin of these fluids and provide evidence for the presence of mantle-derived volatiles in geothermal systems. Helium in geothermal waters is derived from two terrigenous components with distinct isotopic composition (crustal He and mantle He). The continental crust is dominated by isotopically heavy helium (^4He) that has been produced in situ by nuclear reactions (^4He by radioactive decay of uranium and thorium, ^3He by thermal and epithermal neutron capture of lithium) in crustal rocks and minerals. This crustal component has a $^3He/^4He$ ratio of $\sim 2\times10^{-8}$ (Mamyrin and Tolstikhin, 1984; Andrews, 1985). In contrast, the Earth's mantle contains He enriched in the light isotope ^3He that has been inherited from planet formation. The convective mantle as sampled by mid-ocean ridge basalts (MORB) has a $^3He/^4He$ ratio of $\sim 1.1\times10^{-5}$ (Mamyrin and Tolstikhin, 1984; Ozima and Podosek, 2002), though other mantle domains may have higher or lower $^3He/^4He$ ratios. $^3He/^4He$ ratios are often expressed as a multiple of the present-day atmospheric $^3He/^4He$ ratio, R_a, which is 1.39×10^{-6}. Thus, the $^3He/^4He$ ratio of the atmosphere is 1 R_a, that of the crust may vary between ~0.01 and 0.1 R_a, and typical mantle values are ~8 R_a. In the vicinity of the

ACCEPTED MANUSCRIPT

study area, a mantle $^{3}He/^{4}He$ ratio of 7.7 R_a has recently been measured in olivines from the Kula volcanic field (Heineke et al., 2016).

In addition to $^{3}He/^{4}He$ ratios, $CO_2/^{3}He$ ratios are also used to recognize mixing of mantle and crustal fluids (Barry et al., 2013; Karakuş and Şimşek, 2013). Mantle-derived CO_2 gases usually have a $CO_2/^{3}He$ ratio of approximately 2×10^{9} (Marty and Jambon, 1987), which will be preserved unless mixing or fractionation occur during the journey of the mantle gases through the lithosphere (O'Nions and Oxburgh, 1988; Wiersberg et al., 2011; Karakuş and Şimşek, 2013).

In this study, to contribute to the hydrogeochemical conceptual modeling of the geothermal system in the study area, gas geochemistry analyses and helium isotope data were evaluated accordingly. For springs where free gases could be sampled, the total gas compositions are presented in Table 5 together with the helium isotope, $^{4}He/^{20}Ne$ and $CO_2/^{3}He$ ratios. Water samples degassed in the lab were only analyzed for noble gases, therefore no total gas compositions and $CO_2/^{3}He$ ratios are available for them. Air-corrected $^{3}He/^{4}He$ ratios ($(^{3}He/^{4}He)_c$) were calculated according to Craig et al. (1978) and are also given in the same table. According to Table 5, the majority of the gas samples are composed mainly of nitrogen (N_2) with variable amounts of CO_2, Ar, O_2, CH_4, H_2 and He, except for one sample collected from Köyceğiz Lake (SUB-2) in which the major contribution is from CH_4 with considerable contributions of H_2 and O_2. N_2/Ar ratios of the gas samples are up to 119 and are close to the atmospheric value (83). The gas compositions reported here are distinctly different from those reported by Wiersberg et al. (2011) for the Büyük Menderes Graben, where the majority of the samples have CO_2 concentrations > 95%.

The $^{4}He/^{20}Ne$ ratios of the samples range from 0.35 to 130, indicating that contributions from atmospheric He are significant in some samples, but negligible in others when compared to

ACCEPTED MANUSCRIPT

the $^{4}He/^{20}Ne$ ratios of air (~0.319; Sano and Wakita, 1985) or air-saturated water (0.274 at 25 °C; e.g. Ozima and Podosek, 2002) (Table 5). The atmospheric contribution is highest in samples collected from Köyceğiz Lake, where $^{4}He/^{20}Ne$ ratios are close to the ones reported for air, which might be due to admixing of lake water during sampling.

The $(^{3}He/^{4}He)_{c}$ of all samples are above the crustal value (~0.05 R_a), indicating a contribution of mantle origin. A mantle helium component has been reported in Western Anatolia by previous researchers (Güleç, 1988; Güleç and Hilton, 2006; Karakuş and Şimşek, 2013). In fact, Güleç (1988) stated that mantle helium could be observed in a large area in Western Anatolia depending on the distribution of fault systems related to the extensional regime. By using $(^{3}He/^{4}He)_{c}$, which corrects for atmospheric helium contributions, relative fractions of mantle and crustal helium can be calculated using a simple mixing model between mantle and crustal endmembers (Equation 1):

$$\text{Mantle He (\%)} = 100\times [(^{3}He/^{4}He)_{c} - (^{3}He/^{4}He)_{crust}] / [(^{3}He/^{4}He)_{mantle} - (^{3}He/^{4}He)_{crust}]$$

Equation 1

Assuming $(^{3}He/^{4}He)_{crust}$ = 0.02 R_a and $(^{3}He/^{4}He)_{mantle}$ = 8 R_a, mantle He percentages between 2% and 17% are obtained (Table 5). The lowest mantle He contributions were found in the samples from Köyceğiz Lake, whereas the highest ones were observed in springs located on-land in the Dalaman plain near the Mediterranean Sea (THER, MUS, CUR, KAP-2). Small mantle He contributions also occur in on-land springs located near Köyceğiz Lake and the Dalyan Channel (SUL-2, KEL, DEL). The different helium contributions from air, crust and mantle in all samples are visualized in a $^{3}He/^{4}He$ vs. $^{4}He/^{20}Ne$ graph (Fig. 11). For instance, the Köyceğiz Lake samples with the highest atmospheric He contributions plot near air/ASW on the mixing line between ASW and crustal He endmembers (Fig. 11). Likewise, samples with a high crustal He contribution plot near the ASW-crustal He mixing line (Fig. 11). On

ACCEPTED MANUSCRIPT

the other hand, those samples with the highest mantle He contribution are located closer to the mixing line between ASW and mantle He. A relatively high contribution of mantle He in the Dalaman plain suggests that the faults of extensional tectonics in the area promote the escape of gases originating from the deeper parts of the Earth through the brittle parts of the crust, and this affects the geothermal system.

Examining the differences in mantle helium contributions of subaqueous (SUB-2, 3, 4 and SUBC-2) and on-land (SUL-2, KEL, DEL) Köyceğiz Lake samples with the Dalaman plain samples (CUR, MUS, THER, KAP-2) indicates that these samples are products of two different geothermal systems. Köyceğiz Lake on-land samples have relatively high discharge temperatures (between 37 and 40 °C) when compared to Dalaman plain samples (26-30 °C). The $CO_2/^3He$ ratios in free gas samples range from 0.05×10^9 to 1.097×10^9. These ratios are lower than the average ratio reported for the upper mantle ($2x10^9$) (Marty and Jambon, 1987). Moreover, these ratios are much lower than the ones reported by Mutlu et al. (2008), Wiesberg et al. (2011) and Karakuş and Şimşek (2013). This probably reflects the effects of gas fractionation processes (such as degassing and/or dissolution) in the hydrothermal system, which modified the He-CO_2 systematics. A sound discussion of He-CO_2 systematics, however, would require $\delta^{13}C$ data in addition and is beyond the scope of the present study.

4.3.4 Hydrogeochemical model

Our findings from this study enable us to construct a conceptual model (Fig. 12), which shows that fresh water percolates from the fractures, joints, and faults and is heated at depth along the geothermal gradient of the earth. While ascending to the surface from either the sea or lake bottom or on-land via active faults, the waters appear to be mixed with seawater below the sea or lake bottom.

ACCEPTED MANUSCRIPT

The study area is located on the Lycian nappes (Fig. 1), where rock packages are overlain by thrust faults. Generally, faults dip southward. The key point is that the carbonate rocks are pervious, and these rocks are underlain and overlain by the impervious Yeşilbarak nappe and Marmaris nappe, respectively. The southward-dipping nappes force groundwater to flow from north to south (to the Mediterranean). The Yeşilbarak nappe is located at the bottom of all other nappes tectonically; and since it is buried, it crops out in only a very limited area in the study region (Fig. 1). This makes it an impervious mat lying at the bottom of the Lycian nappes. The Marmaris nappe is tectonically the uppermost layer of the Lycian nappes and may be understood as impervious with a peridotite composition. The Gülbahar, Bodrum and Tavas nappes, although differentiated as separate units by Şenel (1997a; 1997b), are made up of carbonate rocks and are sandwiched between these two impervious units, namely the Yeşilbarak nappe at the bottom, and the Marmaris nappe at the top. This arrangement of pervious and impervious nappes creates a somehow confined aquifer in the region (Fig. 12).

The Marmaris Nappe is situated on top of the carbonate nappes, lying as a NW-SE-oriented strip. The carbonate nappes underlie this impervious patch and crop out to the north and to the south of it (Fig. 1). The carbonate units are pervious and known to be karstic in character. The northern outcrop of the karstic nappes can be interpreted as a recharge area of the confined aquifer and the southern outcrop as the discharge area (Fig. 12). The groundwater flow is from the northern highlands towards the southern lowlands, namely the Mediterranean. The southward-dipping tectonic contacts between these units also enable this groundwater movement.

The rainwater precipitated in the northern carbonate highlands travels to the southern low elevation areas below the impervious Marmaris nappe (Fig. 12). The southern boundary of the Marmaris-carbonate nappe units is cut by young normal faults, leading to the formation of a NW-SE lying depression. This depression is filled either by water or by sediments. For

ACCEPTED MANUSCRIPT

example, in the Köyceğiz area it is filled with water forming Köyceğiz Lake. However, around Dalaman, it is filled with alluvium, forming the Dalaman plain. The groundwater traveling from north to south is not able to discharge to the surface due to the overlying Marmaris nappe. However, the heated groundwater immediately emerges at the southern boundary of the Marmaris-carbonate nappe units. This is either due to the normal faults that enable the vertical permeability or to the lack of an impervious cap rock in the south.

The subaqueous hot spring of the Fethiye-Göcek Bay (SUB-7) most probably emerges at the southern Marmaris-carbonate nappe boundary. Since the boundary is covered by seawater and alluvium, its exact location is not visible. We do not know whether the spring emerges exactly at the boundary. The location may be on the carbonate side, since the boundary is covered by alluvium, and there may be a shift where the alluvium is thin enough to allow the groundwater to percolate. Alternatively, the water may emerge on the Marmaris nappe side. The Marmaris nappe may get thinner towards the boundary and become pervious to semi-pervious due to fractures and joints in the rock. In both cases, we can suppose that the hot water emerges not too far away from the boundary.

5. Conclusion

This study aimed to find subaqueous hot springs by making horizontal temperature measurements. Measurements revealed 49 temperature anomalies in the study area and among these anomalies seven of them were confirmed as subaqueous hot springs: three in Köyceğiz Lake, three in the Dalyan Channel, and one in the Fethiye-Göcek Bay. There are no temperature anomalies at the bottom of the Alagöl, Sülüngür and Kocagöl lakes. The temperature of the subaqueous hot springs in the study area ranges between 26 and 29 °C.

According to the chemical analysis results, inland cold waters and stream waters are of the Mg or Ca – HCO3 type. The other samples (subaqueous, lake, channel etc.) are Na-Cl type

ACCEPTED MANUSCRIPT

waters. The on-land fresh waters are of meteoric origin and display highly negative δD and $\delta^{18}O$ values. This is an indication of recharge from inland and high altitudes. However, there is a seawater effect, obvious in the $\delta^{18}O$ and δD values of the remaining waters.

The geology of the region greatly affects the geothermal system in the study area. The Marmaris nappe acts as an impervious cap rock. Especially in the south of the study area, this unit is buried under alluvium and/or lake/seawater. Similarly, the Yeşilbarak nappe also underlies all units as an impervious base rock. Pervious and even karstic carbonate units are sandwiched between these two impervious rocks forming a somehow confined aquifer. The tectonic boundaries between these units are dipping mainly southward. This allows groundwater originating from the northern highlands to travel through the pervious carbonate rocks below the impervious Marmaris nappe. The water travels towards the lowlands in the south, is heated at depth, and mixes with seawater while traveling up through high angle normal faults, it emerges as hot springs from the southern boundary of the carbonate-Marmaris nappe units. The type of hot spring (either on-land or subaqueous) is determined by the local occurrence of alluvium or water. If the boundary is covered by alluvium, like in the case of the Dalaman plain, the hot springs (MUS, THER, KAP, CUR) emerge on land. If the boundary is covered by thin alluvium and a water body (lake/sea/channel), the hot springs emerge either on-land (SUL, DEL, KEL) or subaqueous (SUB-1-7).

According to the total gas analysis results, the majority of the gas samples are composed mainly of nitrogen (N_2) with variable amounts of CO_2, Ar, O_2, CH_4, H_2 and He. N_2/Ar ratios of the gas samples are close to the atmospheric value (up to 119). The $^4He/^{20}Ne$ ratios of the samples indicate that atmospheric contribution is generally negligible, but is significant in some samples such as those taken from Köyceğiz Lake, which might be due to admixing of lake water during sampling. The $(^3He/^4He)_c$ of all samples are above the crustal value (~0.05

ACCEPTED MANUSCRIPT

R_a) which indicate a mantle contribution. According to a mixing model between mantle and crustal endmembers, the lowest mantle He contributions were found in on-land springs located near Köyceğiz Lake (SUL-2, KEL, DEL), whereas the highest ones were observed in springs located around Dalaman plain (THER, MUS, CUR, KAP-2). The differences in mantle helium contributions of subaqueous and on-land Köyceğiz Lake hot springs and Dalaman plain hot springs indicate that they are the products of two different geothermal systems. The $CO_2/^3He$ ratios in free gas samples (0.05×10^9 to 1.097×10^9) are lower than the average ratio reported for the upper mantle ($2x10^9$) and much lower than the ones reported for western Anatolia, which may be attributed to the effects of gas fractionation processes in the hydrothermal system.

S, Cl, Ca, and Sr elements are enriched around Fethiye-Göcek subaqueous hot spring (SUB-7), whereas S, Cl, Br, elements are enriched, Mn element is depleted around Köyceğiz lake subaqueous hot springs. Fluid mineral equilibria calculations reveal that Ca enrichment around SUB-7 is probable from precipitation of aragonite, calcite, dolomite, and fluorite minerals from the hot spring. Sr has a similar atomic structure and chemical properties with Ca. It most probably replaces Ca and displays a parallel anomaly. Cl and S enrichment around both Köyceğiz and Fethiye-Göcek subaqueous hot springs cannot be explained by the fluid mineral equilibria study. S enrichment could be related to biochemical processes.

Acknowledgements

This study was carried out as part of a project supported by The Scientific and Technological Research Council of Turkey (TÜBİTAK, Project Number 112Y137). We acknowledge Nesrin Tüfekçi Avşar for helping with the preparation of plots and spatial distribution maps of sediment elemental ratios. We thank Martin Zimmer for determining the total gas compositions and Enzio Schnabel for performing the noble gas analyses.

ACCEPTED MANUSCRIPT

References

Andrews, J.N., 1985. The isotopic composition of radiogenic helium and its use to study groundwater movement in confined aquifers. Chemical Geology. 49, 339-351.

Arango-Galván, C., Prol-Ledesma, R.M., Flores-Márquez, E.L., Canet, C., Estrada, R.E.V., 2011. Shallow submarine and subaerial, low-enthalpy hydrothermal manifestations in Punta Banda, Baja California, Mexico: Geophysical and geochemical characterization. Geothermics. 40, 102-111.

Avşar, Ö., Kurtuluş, B., Gürsu, S., Gençalioğlu Kuşcu, G., Kaçaroğlu, F., 2016. Geochemical and isotopic characteristics of structurally controlled geothermal and mineral waters of Muğla (SW Turkey). Geothermics. 64, 466–481.

Baba, A., Sözbilir, H., 2012. Source of arsenic based on geological and hydrogeochemical properties of geothermal systems in Western Turkey. Chemical Geology. 334, 364–377.

Balderer, W., Synal, H.-A., 1997. Use of chlorine-36 as a tracer for the evolution of waters in geothermal and tectonically active areas in western Turkey. Nuclear Instruments and Methods in Physics Research Section B: Beam Interactions with Materials and Atoms. 123, 387–393.

Barry, P.H., Hilton, D.R., Fischer, T.P., de Moor, J.M., Mangasini, F., Ramirez, C., 2013. Helium and carbon isotope systematics of cold “mazuku” CO_2 vents and hydrothermal gases and fluids from Rungwe Volcanic Province, southern Tanzania. Chemical Geology. 339, 141-156. http://dx.doi.org/10.1016/j.chemgeo.2012.07.003.

ACCEPTED MANUSCRIPT

Bayarı, C.S., Kazancı, N., Koyuncu, H., Çağlar, S.S., Gökçe, D., 1995. Determination of the origin of the waters of Köyceğiz Lake, Turkey. Journal of Hydrology. 166, 171-191.

Bertani, R., 2015. Geothermal Power Generation in the World 2010-2014 Update Report. Proceedings World Geothermal Congress 2015, Melbourne-Australia.

Bundschuh, J., Maity, J.P., Nath, B., Baba, A., Gunduz, O., Kulp, T.R., Jean, J.-S., Kar, S., Yang, H.-J., Tseng, Y.-J., Bhattacharya, P., Chen, C.-Y., 2013. Naturally occurring arsenic in terrestrial geothermal systems of western Anatolia, Turkey: potential role in contamination of freshwater resources. Journal of Hazardous Materials. 262, 951–959.

Clesceri, L. S., Greenberg, A.E., Trussell, R.R., 1989. Standard Methods for the Examination of Water and Wastewater, Methods, 17th edition, American Public Health Association. Washington, DC.

Corliss J.B., Dymond J., Gordon L.I., Edmond J.M., von Herzen R.P., Ballard, R.D.; Green, K.; Williams, D., Bainbridge, A.; Crane, K., van Andel, T.H., 1979. Submarine thermal sprirngs on the Galapagos rift. Science. 203, 1073-1083.

Craig, H., 1961. Isotopic Variations in Meteoric Waters. Science. 133, 1702-1703.

Craig, H., Lupton, J.E., Horibe, Y., 1978. A mantle helium component in circum-Pacific volcanic gasses: Hakone, the Marianas and Mt Lassen. In: Alexander, E.C., Ozima, M., (Eds). Terrestrial Rare Gases. Japan. Science Society Press, Tokyo, 3-16.

Croudace, I.W., Rindby, A., Rothwell, R.G., 2006. ITRAX: description and evaluation of a new multi-function X-ray core scanner. In: Rothwell, R.G. (Ed.), New Techniques in Sediment Core Analysis, Geological Society London Special Publications. 267, 51-63.

ACCEPTED MANUSCRIPT

De Batist, M., Klerkx, J., Rensbergen, P.V., Vanneste, M., Poort, P., Golmshtok, A.Y., Kremlev, A.A., Khlystov, O.M., Krinitsky, P., 2002. Active hydrate destabilization in Lake Baikal, Siberia? Terra Nova. 14, 436–442.

Duchkov, A.D., Kutasov, I.M., Sokolova, L.S., 2009. Estimating heat flow from an unsteady temperature log of submarine borehole BDP-98 (Lake Baikal). Russian Geology and Geophysics. 50, 131–135.

Esposito, A., Giordano, G., Anzidei, M., 2006. The 2002–2003 submarine gas eruption at Panarea volcano (Aeolian Islands, Italy): Volcanology of the seafloor and implications for the hazard scenario. Marine Geology. 227, 119-134.

Fitzsimons, M.F., Dando, P.R., Hughes, J.A., Thiermann, F., Akoumianaki, I., Pratt, S.M., 1997. Submarine hydrothermal brine seeps off Milos, Greece: Observations and geochemistry. Marine Chemistry. 57, 325-340.

Glasby, G.B., Notsu, K., 2003. Submarine hydrothermal mineralization in the Okinawa Trough, SW of Japan: an overview. Ore Geology Reviews. 23, 299–339.

Gökgöz, A., Tarcan, G., 2006. Mineral equilibria and geothermometry of the Dalaman–Köyceğiz thermal springs, southern Turkey. Applied Geochemistry. 21, 253-268.

Güleç, N., 1988. He-3 distribution in western Turkey. Bulletin of the Mineral Research and Exploration Institute of Turkey. 108, 35–42.

Güleç, N., Hilton, D.R., 2006. Helium and heat distribution in western Anatolia, Turkey: Relationship to active extension and volcanism. Geological Society of America Special Paper. 409, 305-319.

Hall, J., Aksu, A.E., Elitez, I., Yaltırak, C., Çifçi, G. 2014. The Fethiye–Burdur Fault Zone: A

ACCEPTED MANUSCRIPT

component of upper plate extension of the subduction transform edge propagator fault linking Hellenic and Cyprus Arcs, Eastern Mediterranean. Tectonophysics, 635, 80-99.

Hannington, M., Herzig, P., Stoffers, P., Scholten, J., Botz, R., Garbe-Schönberg, D., Jonasson, I.R., Roest, W., 2001. First observations of high-temperature submarine hydrothermal vents and massive anhydrite deposits off the north coast of Iceland. Marine Geology. 177, 199-220.

Heineke, C., Niedermann, S., Hetzel, R., Akal, C., 2016. Surface exposure dating of Holocene basalt flows and cinder cones in the Kula volcanic field (Western Turkey) using cosmogenic ^{3}He and ^{10}Be. Quaternary Geochronology. 34, 81-91.

Hem, J.D., 1985. Study and Interpretation of the Chemical Characteristics of Natural Water. Water Supply Paper 2254, 3rd edition, US Geological Survey, Washington, D.C., pp. 263.

IAEA, 1981. Stable isotope hydrology. Deuterium and oxygen-18 in water cycle, In: Gat, J.R., Gonfiantini, R. (Eds.), International Atomic Energy Agency. Technical Report No. 210, Vienna, 339.

IEA, 2012. World energy outlook 2012 Paris: International Energy Agency.

Italiano, F., Nuccio, P.M., 1991. Geochemical investigations of submarine volcanic exhalations to the east of Panarea, Aeolian Islands, Italy. Journal of Volcanology and Geothermal Research. 46, 125-141.

İlkışık, O.M., 1995. Regional heat flow in western Anatolia using silica temperature estimates from thermal springs. Tectonophysics. 244, 175-184.

ACCEPTED MANUSCRIPT

Karakus, H., Aydin, H., 2016. HNC-Plot: an excel VBA for visualization of helium, nitrogen and CO2 isotope data of crustal and mantle gases, Earth Science Informatics. DOI 10.1007/s12145-016-0272-4

Karakuş, H., Şimşek, Ş., 2013. Tracing deep thermal water circulation systems in the E–W trending Büyük Menderes Graben, western Turkey. Journal of Volcanology and Geothermal Research. 252, 38-52.

Kennedy, B.M., van Soest, M.C., 2007. Flow of mantle fluids through the ductile lower crust: Helium isotope trends. Science. 318, 1433-1436.

Koschinsky, A., Seifert, R., Knappe, A., Schmidt, K., Halbach, P., 2007. Hydrothermal fluid emanations from the submarine Kick'em Jenny volcano, Lesser Antilles island arc. Marine Geology. 244, 129-141.

Kylander, M.E., Ampel, L., Wohlfarth, B., Veres, D., 2011. High-resolution X-ray fluorescence core scanning analysis of Les Echets (France) sedimentary sequence: new insights from chemical proxies. Journal of Quaternary Science. 26, 109-117.

Mamyrin, B.A., Tolstikhin, I.N., 1984. Helium isotopes in Nature. Elsevier, Amsterdam, pp. 273.

Marty, B., Jambon, A., 1987. C/^{3}He in volatile fluxes from the solid Earth: implications for carbon geodynamics. Earth and Planetary Science Letters. 83, 16-26.

McCarthy, K.T., Pichler, T., Price, R.E., 2005. Geochemistry of Champagne Hot Springs shallow hydrothermal vent field and associated sediments, Dominica, Lesser Antilles. Chemical Geology. 224, 55-68.

ACCEPTED MANUSCRIPT

McMurtry, G.M., Sedwick, P.N., Fryer, P., VonderHaar, D.L., Yeh, H.W., 1993. Unusual geochemistry of hydrothermal vents on submarine arc volcanoes: Kasuga Seamounts, Northern Mariana Arc. Earth and Planetary Science Letters. 114, 517-528.

Mertoğlu, O., Şimşek, S., Başarır, N., 2015. Geothermal Country Update Report of Turkey (2005-2010). Proceedings World Geothermal Congress 2010, Bali-Indonesia.

Mertoğlu, O., Şimşek, S., Dağıstan, H., Bakır, N., Doğdu, N., 2010. Geothermal Country Update Report of Turkey (2010-2015). Proceedings World Geothermal Congress 2015, Melbourne-Australia.

Michard, A., Michard, G., Stüben, D., Stoffers, P., Cheminée, J., Binard, N. 1993. Submarine thermal springs associated with young volcanoes: The Teahitia vents, Society Islands, Pacific Ocean. Geochimica et Cosmochimica Acta. 57, 4977-4986.

Michel, F.A., Allen, D.M., Grant, M.B., 2001. Hydrogeochemistry and geothermal characteristics of the White Lake basin, South-central British Columbia, Canada. Geothermics. 31, 169-194.

MTA, 2005. Inventory of Geothermal Resources of Turkey (in Turkish), MTA, Ankara.

Mutlu, H., Güleç, N., 1998. Hydrogeochemical outline of thermal waters and geothermometry applications in Anatolia (Turkey). Journal of Volcanology and Geothermal Research. 85, 495–515.

Mutlu, H., Güleç, N., Hilton, D.R., 2008. Helium-carbon relationships in geothermal fluids of western Anatolia, Turkey. Chemical Geology. 247, 305-321.

ACCEPTED MANUSCRIPT

Niedermann, S., Bach, W., Erzinger, J., 1997. Noble gas evidence for a lower mantle component in MORBs from the southern East Pacific Rise: Decoupling of helium and neon isotope systematics. Geochimica et Cosmochimica Acta. 61, 2697-2715.

O'Nions, R.K., Oxburgh, E.R., 1988. Helium, volatile fluxes and the development of continental crust. Earth and Planetary Science Letters. 90, 331-347.

Ocakoğlu, N., 2011. Investigation of Fethiye-Marmaris Bay (SW Anatolia): seismic and morphologic evidences from the missing link between the Pliny Trench and the Fethiye-Burdur Fault Zone. Geo-Marine Letters. 32, 17-28. doi 10.1007/s00367-011-0234-2.

Ozima, M., Podosek, F.A., 2002. Noble Gas Geochemistry, 2nd edition. Cambridge University Press, Cambridge, pp. 286.

Özgür, N., Çalışkan, T.A., 2013. Active geothermal systems in the Menderes Massif, western Anatolia, Turkey. Procedia Earth and Planetary Science. 7, 652–655.

Parkhurst, D.L., Appelo, C.A.J., 1999. User's Guide to PHREEQC (Version 2-A) Computer Program for Speciation, Batch-Reaction, One-Dimensional Transport, and Inverse Geochemical Calculations.

Pekçetinöz, B., Kayseri, M.S., Eftelioğlu, M., Özel, E., 2009. High-resolution shallow seismic and palynological studies in determining hydrothermal activity in Gülbahçe Bay. Geological Bulletin of Turkey. 52, 325-366. (in Turkish)

Pichler, T., 2005. Stable and radiogenic isotopes as tracers for the origin, mixing and subsurface history of fluids in submarine shallow-water hydrothermal systems. Journal of Volcanology and Geothermal Research. 139, 211-226.

ACCEPTED MANUSCRIPT

Prol-Ledesma, R.M., 2003. Similarities in the chemistry of shallow submarine hydrothermal vents. Geothermics. 32, 639-644.

Prol-Ledesma, R.M., Canet, C., Torres-Vera, M.A., Forrest, M.J., Armienta, M.A., 2004. Vent fluid chemistry in Bahia Concepcion coastal submarine hydrothermal system, Baja California Sur, Mexico. Journal of Volcanology and Geothermal Research. 137, 311-328.

Prol-Ledesma, R.M., Dando, P.R., de Ronde, C.E.J., 2005. Special issue on "shallow-water hydrothermal venting. Chemical Geology. 224, 1–4.

Remsen, C. C., Maki, J. S., Klump, J. V., Aguilar, C., Anderson, P. D., Buchholz, L., Cuhel, R. L., Lovalvo, D., Paddock, R. W., Waples, J., Bruckner, J. C., Schroeder, C. M., 2002. Sublacustrine geothermal activity in Yellowstone Lake: studies past and present. In: Yellowstone Lake: Hotbed of Chaos or Reservoir of Resilience?: Proceedings of the 6th Biennial Scientific Conference on the Greater Yellowstone Ecosystem. Anderson, R. J., Harmon, D. (Eds.), pp. 192–212.

Ronde, C.E.J., Stoffers, P., Garbe-Schönberg, D., Christenson, B.W., Jones, B., Manconi, R., Browne, P.R.L., Hissmann, K., Botz, R., Davy, B.W., Schmitt, M., Battershill, C.N., 2002. Discovery of active hydrothermal venting in Lake Taupo. Journal of Volcanology and Geothermal Research. 115, 257-275.

Sano, Y., Wakita, H., 1985. Geographical distribution of 3He/4He ratios in Japan: Implications for arc tectonics and incipient magmatism. Journal of Geophysical Research. 90, 8729-8741:

ACCEPTED MANUSCRIPT

Suarez-Arriaga, M.C., Bundschuh, J., Samaniego, F., 2014. Assessment of submarine geothermal resources and development of tools to quantify their energy potentials for environmentally sustainable development. Journal of Cleaner Production. 83, 21-32.

Süer, S., Güleç, N., Mutlu, H., Hilton, D.R., Çifter, C., Sayın, M., 2008. Geochemical monitoring of geothermal waters (2002–2004) along the North Anatolian Fault Zone, Turkey: spatial and temporal variation and relationship to seismic activity. Pure and Applied Geophysics. 165, 17–43.

Şenel, M., 1997a. Geological Map Series of Turkey 1:100 000 scale. No. 1, Geologic Map of Fethiye L7 Quadrangle. General Directorate of Mineral Research and Exploration, Geological Research Department, Ankara (in Turkish).

Şenel, M., 1997b. Geological Map Series of Turkey 1:100 000 scale. No. 2, Geologic Map of Fethiye L8 Quadrangle. General Directorate of Mineral Research and Exploration, Geological Research Department, Ankara (in Turkish).

Tarcan, G., 2005. Mineral saturation and scaling tendencies of waters discharged from wells (>150°C) in geothermal areas of Turkey. Journal of Volcanology and Geothermal Research. 142, 263–283.

Tüfekçi, N., Süzen, M.L., Güleç, N., 2010. GIS based geothermal potential assessment: A case study from Western Anatolia, Turkey. Energy. 35, 246-261.

Valsami-Jones, E., Baltatzis, E., Bailey, E.H., Boyce, A.J., Alexander, J.L., Magganas, A., Anderson, L., Waldron, S., Ragnarsdottir, K.V., 2005. The geochemistry of fluids from an active shallow submarine hydrothermal system: Milos island, Hellenic Volcanic Arc. Journal of Volcanology and Geothermal Research. 148, 130-151.

ACCEPTED MANUSCRIPT

Vengosh, A., Helvaci, C., Karamanderesi, İ.H., 2002. Geochemical constraints for the origin of thermal waters from western Turkey. Applied Geochemistry. 17, 163–183.

Wiersberg, T., Süer, S., Güleç, N., Erzinger, J., Parlaktuna, M., 2011. Noble gas isotopes and the chemical composition of geothermal gases from the eastern part of the Büyük Menderes Graben (Turkey). Journal of Volcanology and Geothermal Research. 208, 112-121.

Williams, D.L., 1976. Submarine Geothermal Resources. Journal of Volcanology and Geothermal Research. 1, 85-100.

Williams, D.L., Von Herzen, R.P., Sclater, J.G., Anderson, R.N., 1974. The Galapagos spreading centre: lithospheric cooling and hydrothermal circulation. Geophysical Journal International. 38(3), 587-608.

Yağmurlu, F., Bozcu, M., Şentürk, M., 2005. Investigation of seismotectonic characteristics of Burdur Faults in between Burdur and Fethiye region. TÜBİTAK report, Project No. 101Y027. (in Turkish).

Yamanaka, T., Maeto, K., Akashi, H., Ishibashi, J., Miyoshi, Y., Okamura, K., Noguchi, T., Kuwahara, Y., Toki, T., Tsunogai, U., Ura, T., Nakatani, T., Maki, T., Kubokawa, K., Chiba H., 2013. Shallow submarine hydrothermal activity with significant contribution of magmatic water producing talc chimneys in the Wakamiko Crater of Kagoshima Bay, southern Kyushu, Japan. Journal of Volcanology and Geothermal Research. 258, 74–84.

Figure Captions

Fig. 1. Geological map of the study region (modified from Şenel, 1997a; Şenel, 1997b) with water sampling locations indicated. Sample labels are given in Table 1 along with sample

ACCEPTED MANUSCRIPT

information. Fethiye-Burdur and Pliny-Strabo fault zones are shown on the upper right inset map as FBFZ and PSFZ, respectively (Hall et al., 2014).

Fig. 2. Physicochemical measurement routes in (a) Dalyan Channel, Köyceğiz, Alagöl, and Sülüngür Lakes; (b) Fethiye-Göcek Bay and Kocagöl Lake (in the west). Bathymetry maps of (c) Köyceğiz Lake and (d) Fethiye-Göcek Bay.

Fig. 3. Locations of 233 gravity cores collected from a) Köyceğiz Lake, b) Dalyan Channel, and c) Fethiye-Göcek Bay. The white dots are "Cold Location Cores" (CLC), while the red dots are "Hot Location Cores" (HLC). The insets are close-up views around the HLCs.

Fig. 4. a) An example illustration ofthe comparison of the mean Sr/Ti ratios in the HLCs and CLCs from the Fethiye-Göcek Bay. The mean of the Sr/Ti ratio in HLCs (i.e., around the subaqueous hot spring) is significantly higher than the mean of the CLCs (by approximately 4σ), which implies that sediments around the subaqueous hot spring are enriched in Sr. b) Spatial distribution of the Sr/Ti ratio over the Fethiye-Göcek Bay. The maximum around the F-71 core also implies the presence of another subaqueous hot spring around that location.

Fig. 5. Matrices illustrating the magnitude of deviations between absolute means of HLCs and CLCs for all possible elemental ratios; a) Köyceğiz Lake, b) Dalyan Channel, c) Fethiye-Göcek Bay. For example, in the Köyceğiz matrix, the cell at the intersection of the 4^{th} column and the 5^{th} row shows that the mean Cl/K ratio of the HLCs is 2.5σ higher than the mean Cl/K ratio of the CLCs.

Fig. 6. Plots and spatial distributions of the mean ratios of enriched elements in Köyceğiz Lake (left) and Fethiye-Göcek Bay (right). The gray lines in the plots stand for individual elemental ratios, while the black and red lines indicate the mean of these ratios for the CLCs and HLCs, respectively. The horizontal lines on the graphs indicate ±1σ boundaries for CLCs.

ACCEPTED MANUSCRIPT

Note the significant difference in elemental enrichments in the southern basin of Köyceğiz Lake. The basinwide difference is attributed to the lack of tributaries in the southern basin, which enhances the effect of subaqueous hot springs on the overall sediment chemistry.

Fig. 7. Piper diagram of waters.

Fig. 8. Cl vs. Total Dissolved Solids (TDS) graph.

Fig. 9. Temperature vs. Saturation Index (SI) diagrams for samples SUB-1 and SUB-7.

Fig. 10. $\delta^{18}O$ vs. δD diagram of waters [GMWL: **G**lobal **M**eteoric **W**ater **L**ine (Craig, 1961); MMWL: **M**editerranean **M**eteoric **W**ater **L**ine (IAEA, 1981)] (a) wet, (b) dry season measurements.

Fig. 11. $^{3}He/^{4}He$ (R_a) versus $^{4}He/^{20}Ne$ graph for hydrothermal fluids and gases. Binary mixing lines between air saturated water (ASW) ($^{3}He/^{4}He$ =1 R_a), mantle ($^{3}He/^{4}He_{mantle}$=8 R_a) and crustal ($^{3}He/^{4}He_{crust}$ =0.02 R_a) endmember compositions, 1% and 20% air-mantle mixing lines (mantle %) and 1%, 10%, 20% and 50% air proportions (air %) are also presented herein. The graph was prepared using the HNC-Plot application (Karakuş and Aydın, 2016).

Fig. 12. Sketch of a conceptual hydrogeochemical model for the study area. Not to scale. Modified from Gökgöz and Tarcan (2006) and Avşar et al. (2016).

Supplementary Fig. 1. (a) Temperature and probe depth measurements taken around the submarine hot springs. The anomalies of SUB-1, SUB-4, SUB-5 and SUB-7 hot springs are marked by circles. Temperature anomaly at 18:02:14 on 26.08.2013 indicates SUB-7 hot spring. A second measurement on 31.08.2014 verified the existence of SUB-7 hot spring. See the anomaly at 15:21:00 marked by a circle. (b) Sonar profiles used to detect SUB-2 and SUB-3.

ACCEPTED MANUSCRIPT

Supplementary Fig. 2. Optical and radiographic images of the artificial cores composed of the top 3-5 cm sediments from 233 gravity cores. Labels and coordinates of each gravity core are presented as well. “K”: Köyceğiz, “D”: Dalyan, “F”: Fethiye-Göcek, and “I”: İnlice Bay in Fethiye-Göcek Bay.

Supplementary Fig. 3. Plots of elemental ratios based on the standardized “kcps” values for (a) Köyceğiz Lake, (b) Dalyan Channel, (c) Fethiye-Göcek Bay.

Supplementary Fig. 4. Spatial distribution maps of elemental ratios over the study area. (a) Köyceğiz Lake, (b) Dalyan Channel, (c) Fethiye-Göcek Bay.

ACCEPTED MANUSCRIPT

ACCEPTED MANUSCRIPT

Table 1. Sampling locations and water parameters.

	Type	Location	Sample label	Sampling date	Coordinates (UTM / ED50)		Temp. (°C)	TDS[a] (ppm)	EC[b] (mS/cm)	pH
					E	N				
1	On-land hot	Sultaniye-1	SUL-1	01.06.2014	642788	4082305	24.30	26438	18.700	6.92
2	On-land hot	Sultaniye-2	SUL-2	21.06.2014	642853	4082265	39.93	27127	44.250	6.74
3	On-land hot	Sultaniye-3	SUL-3	21.06.2014	642805	4082293	41.04	28163	44.100	6.70
4	On-land hot	Kelgirme	KEL	02.07.2014	645593	4078489	37.71	27302	27.410	6.76
5	On-land hot	Delibey	DEL	21.06.2014	644921	4080156	38.98	28841	44.390	6.75
6	On-land hot	Çürükardı	CUR	22.06.2014	656671	4065767	29.27	23029	24.400	6.43
7	On-land hot	Musalar	MUS	22.06.2014	654393	4068427	26.58	23031	25.630	6.5
8	On-land hot	Thermemaris	THER	26.06.2014	660168	4062670	26.60	20042	22.740	6.55
9	On-land hot	Kapukargın-1	KAP-1	22.06.2014	661828	4066361	30.02	19505	22.590	6.44
10	On-land hot	Kapukargın-2	KAP-2	22.06.2014	661869	4066291	30.16	21434	22.410	6.43
11	Subaqueous hot	Köyceğiz Lake	SUB-1	05.09.2013	642409	4082916	29.47	6671	11648	-
12	Subaqueous hot	Köyceğiz Lake	SUB-2	28.06.2014	642725	4082889	26.29	5629	5.102	8.67
13	Subaqueous hot	Köyceğiz Lake	SUB-3	28.06.2014	643870	4081804	26.17	7200	4.951	8.69
14	Subaqueous hot	Dalyan Channel	SUB-4	28.06.2014	645593	4079204	27.37	24354	34.406	8.23
15	Subaqueous hot	Dalyan Channel	SUB-5	28.06.2014	645679	4078895	27.47	21572	33.951	8.26
16	Subaqueous hot	Dalyan Channel	SUB-6	28.06.2014	646005	4078338	27.61	20547	30.134	8.25
17	Subaqueous hot	Fethiye-Göcek Bay	SUB-7	28.06.2014	675787	4066071	27.19	6671	57.734	8.35
18	On-land cold	Köyceğiz	COLD-1	21.06.2014	650135	4091604	15.03	302	0.305	8.65
19	On-land cold	Köyceğiz	COLD-2	21.06.2014	654921	4089336	18.72	611	0.627	7.92
20	On-land cold	Sultaniye Village	COLD-3	26.06.2014	641110	4084397	23.77	718	0.709	8.57
21	On-land cold	Çandır Village	COLD-4	21.06.2014	642438	4077514	17.94	409	0.470	7.02
22	On-land cold	İnlice Village	COLD-5	26.06.2014	675818	4067938	18.47	613	0.800	7.32
23	Subaqueous cold	Köyceğiz Lake	SUBC-1	28.06.2014	651338	4091283	25.07	2581	2.780	8.84
24	Subaqueous cold	Köyceğiz Lake	SUBC-2	28.06.2014	646048	4084218	27.70	2802	3.698	8.71
25	Stream	Namnam Stream	NAM	22.06.2014	644396	4087801	22.72	473	0.539	8.12
26	Stream	Yuvarlakçay Stream	YUV	22.06.2014	650966	4086369	20.07	540	0.594	7.83
27	Lake	Köyceğiz Lake	KOY-1	28.06.2014	650033	4089319	27.60	2917	3.635	8.88
28	Lake	Köyceğiz Lake	KOY-2	28.06.2014	648020	4086829	27.52	2865	3.702	8.91

ACCEPTED MANUSCRIPT

29	Lake	Köyceğiz Lake	KOY-3	28.06.2014	645751	4084993	27.84	2849	3.848	8.89
30	Lake	Köyceğiz Lake	KOY-4	28.06.2014	643216	4083815	28.60	3247	3.940	8.82
31	Lake	Köyceğiz Lake	KOY-5	28.06.2014	645147	4082863	27.73	3258	4.056	8.82
32	Lake	Alagöl Lake	ALA-1	28.06.2014	643431	643431	32.15	27337	50.565	8.18
33	Lake	Alagöl Lake	ALA-2	10.09.2013	643727	4076043	32.90	37065	53.285	8.22
34	Lake	Sülüngür Lake	SULG-1	01.07.2014	645231	4073821	28.92	5254	35.698	8.26
35	Lake	Sülüngür Lake	SULG-2	01.07.2014	646606	4072741	29.75	10498	35.138	8.44
36	Lake	Kocagöl Lake	KOC	22.06.2014	663646	4061694	28.51	4621	7.261	8.31
37	Channel	Dalyan Channel	DAL-1	28.06.2014	645606	4079815	28.09	3433	5.316	8.75
38	Channel	Dalyan Channel	DAL-2	28.06.2014	645861	4076524	27.83	21549	37.126	8.21
39	Sea	Fethiye-Göcek Bay	GOC-1	02.06.2014	675724	4063884	21.13	41133	57.562	8.38
40	Sea	Fethiye-Göcek Bay	GOC-2	05.06.2014	669676	4061469	22.10	41528	56.654	8.38
41	Sea	Fethiye-Göcek Bay	GOC-3	03.06.2014	674596	4056408	22.71	41526	57.482	8.38

[a] Total dissolved solids
[b] Electrical conductivity

ACCEPTED MANUSCRIPT

ACCEPTED MANUSCRIPT

Table 2. Major ion concentrations of the waters. CBE: Charge Balance Error.

Sample No	Ca (ppm)	Mg (ppm)	Na (ppm)	K (ppm)	HCO_3 (ppm)	SO_4 (ppm)	Cl (ppm)	CBE (%)	Type
SUL-1	1994	946	6510	284	302	1453	14874	1.30	Na - Cl
SUL-2	2294	1280	6216	355	302	2136	14453	4.27	Na - Cl
SUL-3	2588	1289	6123	389	302	2233	15067	3.26	Na - Cl
KEL	2478	1262	6028	348	178	2068	14843	3.38	Na - Cl
DEL	2928	1321	6161	377	308	2285	15262	4.55	Na - Cl
CUR	2055	895	5009	269	847	934	12894	0.24	Na - Cl
MUS	2059	975	5353	212	900	991	12431	4.16	Na - Cl
THER	1881	907	4403	196	794	804	10932	3.53	Na - Cl
KAP-1	2183	833	4012	232	865	895	10348	4.50	Na - Cl
KAP-2	1857	785	4815	218	882	948	11749	0.50	Na - Cl
SUB-1	378	414	1514	64	302	596	3369	3.36	Na - Cl
SUB-2	414	369	1076	79	320	477	2863	1.93	Na - Cl
SUB-3	414	451	1636	82	317	498	3740	4.60	Na - Cl
SUB-4	916	1378	5929	318	255	1743	13752	-0.47	Na - Cl
SUB-5	944	1020	5962	283	267	1481	11551	4.72	Na - Cl
SUB-6	946	904	5534	304	267	1440	11081	3.12	Na - Cl
SUB-7	1739	2400	10293	532	184	2948	23037	2.05	Na - Cl
COLD-1	17.14	35.09	5.79	0.62	219	2.57	4.04	2.67	Mg - HCO3
COLD-2	16.59	84.70	6.25	0.70	444	5.01	6.91	3.18	Mg - HCO3
COLD-3	8.74	114.64	6.58	0.38	503	4.15	8.60	4.11	Mg - HCO3
COLD-4	86.03	6.03	11.58	0.99	267	8.17	16.39	2.76	Ca - HCO3
COLD-5	84.13	31.94	35.51	1.60	361	16.35	49.76	4.21	Ca - HCO3
SUBC-1	127	190	513	29	320	172	1204	2.34	Na - Cl
SUBC-2	121	196	617	31	326	184	1305	3.92	Na - Cl
NAM	16.04	70.49	5.18	0.77	354	4.22	6.31	2.09	Mg - HCO_3
YUV	77.87	40.11	5.57	0.81	302	45.43	5.79	3.38	Ca - HCO_3
KOY-1	108	204	681	34	284	185	1375	4.55	Na - Cl
KOY-2	100	207	653	30	290	182	1358	3.66	Na - Cl
KOY-3	96	207	661	30	314	180	1335	4.80	Na - Cl
KOY-4	100	224	804	34	264	207	1566	4.98	Na - Cl
KOY-5	104	221	806	36	267	207	1568	4.92	Na - Cl
ALA-1	1164	1626	7038	347	267	1604	15173	4.01	Na - Cl
ALA-2	1669	2056	9747	494	207	2616	20174	4.61	Na - Cl
SULG-1	179	332	1286	67	302	352	2702	2.81	Na - Cl
SULG-2	298	603	2847	141	290	690	5585	4.01	Na - Cl
KOC	210	204	1232	49	267	261	2355	3.21	Na - Cl
DAL-1	113	204	893	36	267	218	1647	4.84	Na - Cl
DAL-2	1715	1262	4843	215	302	1112	12023	4.84	Na - Cl
GOC-1	1426	2454	11037	629	130	2752	22574	4.83	Na - Cl
GOC-2	1529	2450	11166	555	178	2768	22782	4.94	Na - Cl
GOC-3	1378	2486	11056	554	184	2812	22940	3.94	Na - Cl

ACCEPTED MANUSCRIPT

Table 3. Trace element concentrations of the waters. Pikcogram/gram

Sample No	Al (ppb)	As (ppb)	Ba (ppb)	Br (ppm)	Cr (ppb)	Cu (ppb)	F (ppm)	Fe (ppb)	Mn (ppb)	Ni (ppb)	Se (ppb)
Detection Limit	0.3	0.025	0.002	0.01	0.003	0.02	0.01	0.05	0.03	0.03	0.01
SUL-1	775	258	165	31	96	<0.02	6	3279	<0.03	125	202
SUL-2	<0.3	365	109	42	99	<0.02	11	2963	<0.03	165	334
SUL-3	<0.3	234	116	44	110	<0.02	15	3052	<0.03	49	473
KEL	<0.3	405	98	36	118	440	8	3323	<0.03	23	357
DEL	<0.3	290	104	47	130	13070	7	3574	<0.03	87	309
CUR	<0.3	319	95	22	119	<0.02	10	3439	<0.03	45	235
MUS	<0.3	121	80	25	136	<0.02	8	4602	102	35	311
THER	<0.3	216	119	18	141	<0.02	10	3897	<0.03	24	320
KAP-1	<0.3	373	97	20	154	<0.02	19	4924	115	54	210
KAP-2	<0.3	375	103	29	165	<0.02	15	5895	<0.03	47	324
SUB-1	<0.3	103	34	9	60	<0.02	1	1451	<0.03	<0.1	79
SUB-2	<0.3	98	20	5	70	<0.02	<0.01	1851	<0.03	<0.1	68
SUB-3	<0.3	113	33	8	72	<0.02	1	2025	<0.03	<0.1	72
SUB-4	<0.3	386	47	41	236	<0.02	2	11100	<0.03	50	249
SUB-5	<0.3	186	36	34	131	<0.02	4	3558	<0.03	<0.1	223
SUB-6	<0.3	253	36	36	183	<0.02	1	4925	<0.03	<0.1	267
SUB-7	<0.3	229	17	67	175	<0.02	10	4350	<0.03	<0.1	350
COLD-1	<0.3	9	24	<0.01	11	<0.02	<0.01	134	<0.03	<0.1	2
COLD-2	<0.3	6	1	<0.01	9	<0.02	<0.01	125	<0.03	<0.1	2
COLD-3	<0.3	33	2	<0.01	26	<0.02	<0.01	614	<0.03	20	11
COLD-4	<0.3	8	97	<0.01	3	<0.02	<0.01	45	<0.03	<0.1	3
COLD-5	<0.3	6	84	<0.01	4	<0.02	<0.01	43	<0.03	<0.1	<0.1
SUBC-1	<0.3	28	38	4	33	<0.02	1	1015	<0.03	<0.1	28
SUBC-2	<0.3	44	33	4	31	<0.02	<0.01	768	<0.03	2	31
NAM	26	1	11	<0.01	4	<0.02	<0.01	<0.05	<0.03	2	<0.1
YUV	<0.3	4	105	<0.01	6	<0.02	<0.01	66	<0.03	1	3
KOY-1	<0.3	50	39	4	26	<0.02	2	655	<0.03	3	61
KOY-2	<0.3	48	95	4	27	31	<0.01	735	<0.0	2	49

ACCEPTED MANUSCRIPT

									3		
KOY-3	<0.3	47	34	4	30	<0.02	<0.01	726	<0.03	5	47
KOY-4	<0.3	41	36	4	39	<0.02	<0.01	1271	<0.03	9	50
KOY-5	<0.3	55	37	5	30	<0.02	1	776	<0.03	7	42
ALA-1	<0.3	215	54	41	291	<0.02	11	10280	<0.03	101	326
ALA-2	<0.3	290	26	62	173	<0.02	3	4713	<0.03	<0.1	392
SULG-1	<0.3	47	37	8	25	<0.02	3	638	<0.03	7	64
SULG-2	<0.3	140	44	16	56	<0.02	4	1394	<0.03	12	122
KOC	<0.3	63	76	6	37	<0.02	1	1470	<0.03	7	45
DAL-1	<0.3	66	37	5	28	<0.02	<0.01	771	<0.03	1	45
DAL-2	<0.3	282	69	38	210	<0.02	3	8355	<0.03	32	164
GOC-1	<0.3	266	30	68	173	549	3	5710	<0.03	17	424
GOC-2	<0.3	251	12	70	175	<0.02	5	5171	<0.03	98	344
GOC-3	<0.3	432	25	67	162	<0.02	2	4111	<0.03	18	430

ACCEPTED MANUSCRIPT

ACCEPTED MANUSCRIPT

Table 4. Results from the stable isotope analysis of the waters.

Sample no	DRY		WET		DIFFERENCE	
	$\delta^{18}O$ (‰)	δD (‰)	$\delta^{18}O$ (‰)	δD (‰)	$\delta^{18}O$ (‰)	δD (‰)
SUL-1	-2.74	-14.0	-4.67	-24.7	1.93	10.8
SUL-2	-0.68	-5.9	-1.72	-6.1	1.04	0.1
SUL-3	-0.58	-6.4	-1.46	-6.9	0.88	0.5
KEL	-1.10	-6.6	-1.69	-7.7	0.59	1.1
DEL	-0.73	-2.7	-1.72	-6.3	0.99	3.7
CUR	-4.53	-24.9	-4.91	-28.9	0.38	4.0
MUS	-4.22	-25.5	-4.63	-28.5	0.41	3.0
THER	-4.53	-27.4	-4.97	-26.5	0.44	-1.0
KAP-1	-4.94	-25.7	-5.15	-30.1	0.21	4.4
KAP-2	-1.08	-3.7	-5.31	-30.0	4.23	26.3
SUB-1	-3.25	-14.8				
SUB-2	-3.28	-17.7	-4.59	-22.9	1.31	5.1
SUB-3	-3.28	-16.5	-4.46	-25.8	1.18	9.3
SUB-4	-0.80	-1.3	-1.86	-9.2	1.06	7.9
SUB-5	-1.38	-5.1	-1.98	-9.7	0.60	4.6
SUB-6	-1.20	-5.1	-1.20	-5.7	0.00	0.5
SUB-7	1.46	7.6	0.43	6.8	1.03	0.8
COLD-1	-6.65	-34.6	-7.25	-32.5	0.60	-2.2
COLD-2	5.86	-28.4	-6.01	-33.4	11.87	5.0
COLD-3	-5.39	-25.0	-6.14	-24.5	0.75	-0.6
COLD-4	-5.47	-24.9	-5.81	-30.3	0.34	5.4
COLD-5	-5.85	-27.4	-6.31	-27.6	0.46	0.3
SUBC-1	-3.47	-16.9	-4.41	-26.6	0.94	9.6
SUBC-2	-3.48	-19.6	-3.82	-22.5	0.34	2.9
NAM	-	-	-6.07	-31.0	-	-
YUV	-6.31	-34.5	-6.89	-32.1	0.58	-2.4
KOY-1	-3.37	-18.0	-4.02	-24.5	0.65	6.5
KOY-2	-3.36	-18.1	-4.39	-25.7	1.03	7.6
KOY-3	-3.03	-17.9	-4.09	-23.5	1.06	5.6
KOY-4	-3.19	-16.4	-4.29	-21.9	1.10	5.5
KOY-5	-3.09	-15.8	-4.48	-20.5	1.39	4.7
ALA-1	-0.48	-3.07	-1.93	-10.4	1.45	7.3
ALA-2	0.78	2.76	-0.27	1.8	1.05	0.9
SULG-1	-3.23	-17.0	-0.88	-3.9	-2.35	-13.1
SULG-2	-2.62	-13.9	-1.22	-6.3	-1.40	-7.7
KOC	-0.23	-3.0	-1.01	-5.1	0.78	2.1
DAL-1	-3.11	-18.0	-4.38	-20.1	1.27	2.0
DAL-2	-2.33	-13.1	-1.82	-8.3	-0.51	-4.8
GOC-1	1.63	11.6	0.80	4.3	0.83	7.2
GOC-2	1.49	10.5	0.55	4.4	0.94	6.2
GOC-3	1.46	10.0	0.48	6.6	0.98	3.5

ACCEPTED MANUSCRIPT

Table 5. Total gas composition, $^{3}He/^{4}He$, $^{4}He/^{20}Ne$ and $CO_2/^{3}He$ ratios for free gas samples and $^{3}He/^{4}He$ and $^{4}He/^{20}Ne$ ratios for dissolved gases from hot springs. Error limits are 2σ.

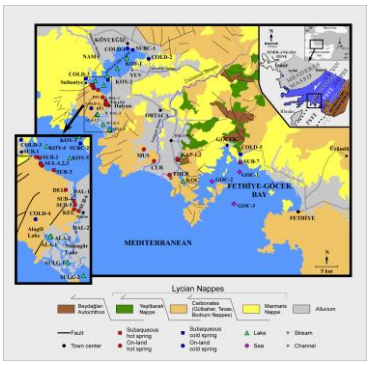
Sample ID	Sample type	Sampling date	Ar	CH_4	CO_2	N_2	O_2	He	H_2	N_2/CH_4	N_2/Ar	$CO_2/^{3}He$	$^{4}He/^{20}Ne$	$^{4}He/^{20}Ne$ error	$^{3}He/^{4}He$ (Ra)	$^{3}He/^{4}He$ (Ra) error	$(^{3}He/^{4}He)_c$	$(^{3}He/^{4}He)_c$ (R_a) error	Mantle Helium[b] (%)
			(%)	(%)	(%)	(%)	(%)	ppm	(ppm)			(*10^9)			(R_a)		(R_a)		
SUL-2	Free Gas	7/8/2014	1.17	0.1	5.1	93	0.2	220	165	650	79	1.026	34.6	±1.7	0.163	±0.012	0.156	±0.012	2
KEL	Free Gas	7/17/2014	1.17	0	4.6	92	2.5	180	165		78	1.097	30.5	±1.6	0.168	±0.012	0.160	±0.012	2
DEL	Free Gas	7/8/2014	1	0.1	4.5	94	0	210	300	870	94	0.932	35.4	±1.8	0.165	±0.011	0.158	±0.011	2
MUS	Free Gas	7/9/2014	0.76	0	4.2	91	4.3	420	50	9100	119	0.050	118.7	±6.0	1.426	±0.027	1.427	±0.027	18
THER	Free Gas	7/9/2014	0.94	0	10.3	88	0.3	460	170	8800	94	0.118	92.6	±4.7	1.365	±0.029	1.366	±0.029	17
KAP-2	Free Gas	7/9/2014	0.72	0.1	21.4	78	0.3	440	135	1270	108	0.255	130.1	±6.5	1.372	±0.027	1.373	±0.027	17
SUB-2	Free Gas	7/17/2014	0.36	62	0.19	34	3.1	28	1460	0.55	96	0.150	1.75	±0.09	0.330	±0.027	0.194	±0.036	2
SUB-3	Dissolved Gas	7/17/2014											0.352	±0.023	0.822	±0.058	<0.61		<7.4
CUR	Dissolved Gas	7/9/2014											89.0	±4.5	1.408	±0.041	1.409	±0.041	17
SUB-4	Dissolved Gas	7/17/2014											0.937	±0.051	0.419	±0.033	0.152	±0.062	2
SUBC-2	Dissolved Gas	7/17/2014											0.466	±0.028	0.651	±0.032	0.05	±0.19	1
Atmosphere/ ASW (25 °C)											83/38		0.319/0.274						

[a] assuming $(^{4}He/^{20}Ne)_{air} = 0.295 \pm 0.025$, i.e. a range including air (0.319; Sano and Wakita, 1985) and ASW (25°C) (0.274; Ozima and Podosek, 2002)

[b] assuming $(^{3}He/^{4}He)_{crust} = 0.02\ R_a$ and $(^{3}He/^{4}He)_{mantle} = 8\ R_a$

ACCEPTED MANUSCRIPT

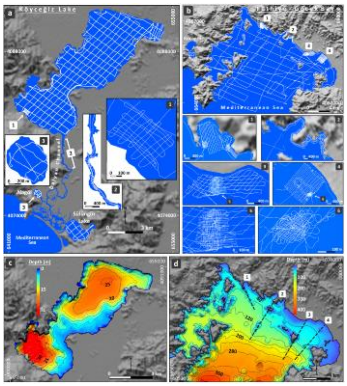
Fig. 1



ACCEPTED MANUSCRIPT

ACCEPTED MANUSCRIPT

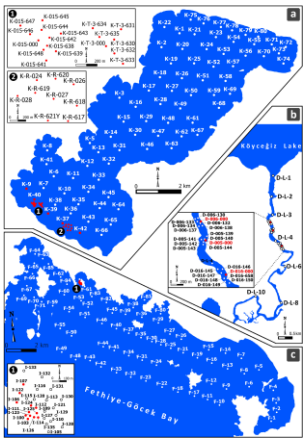
Fig. 2



ACCEPTED MANUSCRIPT

ACCEPTED MANUSCRIPT

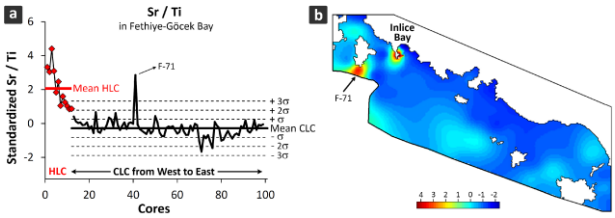
Fig. 3



ACCEPTED MANUSCRIPT

ACCEPTED MANUSCRIPT

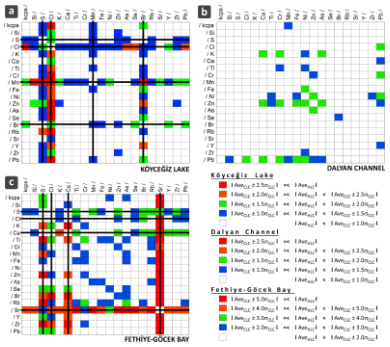
Fig. 4



ACCEPTED MANUSCRIPT

ACCEPTED MANUSCRIPT

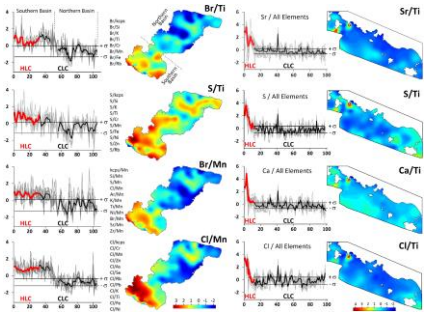
Fig. 5



ACCEPTED MANUSCRIPT

ACCEPTED MANUSCRIPT

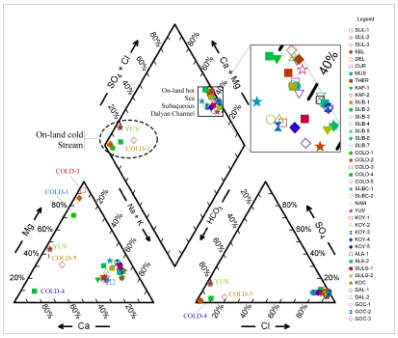
Fig. 6



ACCEPTED MANUSCRIPT

ACCEPTED MANUSCRIPT

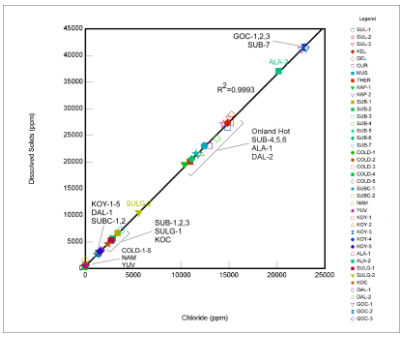
Fig. 7



ACCEPTED MANUSCRIPT

ACCEPTED MANUSCRIPT

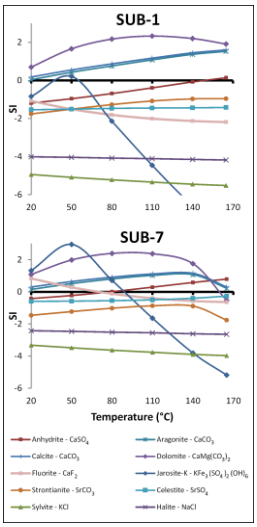
Fig. 8



ACCEPTED MANUSCRIPT

ACCEPTED MANUSCRIPT

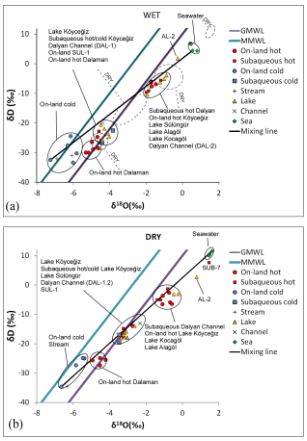
Fig. 9



ACCEPTED MANUSCRIPT

ACCEPTED MANUSCRIPT

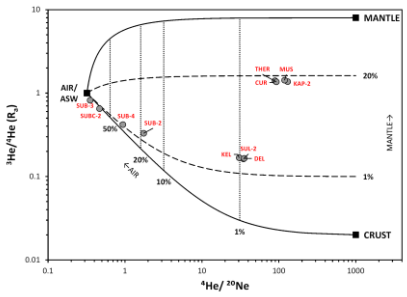
Fig. 10



ACCEPTED MANUSCRIPT

ACCEPTED MANUSCRIPT

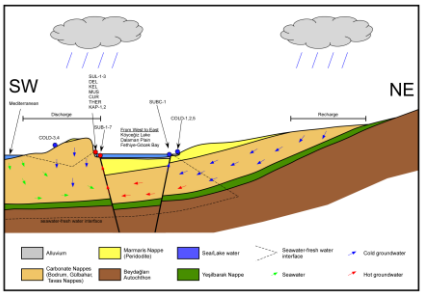
Fig. 11



ACCEPTED MANUSCRIPT

ACCEPTED MANUSCRIPT

Fig. 12



ACCEPTED MANUSCRIPT

ACCEPTED MANUSCRIPT

Highlights

- Horizontal temperature measurements were used to detect 7 subaqueous hot springs.
- Chemical and isotopic properties of waters point to seawater mixing at deep levels.
- Sediments around the subaqueous hot spring are enriched in certain elements.
- Highest He contributions are found in samples from the Dalaman plain.

ACCEPTED MANUSCRIPT